J. COMBIN. MATH. COMBIN. COMPUT. 127b (2025) 2361--2382

Journal of Combinatorial Mathematics
and Combinatorial Computing
www.combinatorialpress.com/jcmcc

Study on the role of electromagnetic waves in quantum entanglement and quantum state transport based on constrained optimization algorithm

Hao Zhang[1,✉]

[1] *Weinan Normal University, Weinan, Shaanxi, 714099, China*

ABSTRACT
In the current fields of quantum information processing and quantum computing, fast and accurate quantum state manipulation and preparation have been of keen interest to researchers, and their potential applications are mainly in quantum measurement, quantum information, quantum communication, and quantum sensing. In this paper, the Hilbert space of a bipartite state system is unfolded by four Bell state entanglement bases and the result is projected to the subsystem to obtain a mixed state. A quantum approximation algorithm is proposed to provide a solution to the combinatorial optimization problem, and based on the workflow of the quantum approximation optimization algorithm, an improvement is proposed to the quantum approximation optimization algorithm to solve the constrained problem using the quadratic unconstrained binary optimization method. Based on the theory of cavity magnetism, the hybrid quantum system model is constructed, and the calculation method of Hamiltonian quantity is proposed. Combined with the quantum entanglement optimal path calculation of UQAOA algorithm, the optimal value of time-microwave entanglement E_{ac} is obtained at r=0.234, so the compression parameter r=0.2 is used in the calculation. Based on the UQAOA algorithm for the analysis of the transmission characteristics of the generated OMA wave in air and the transmission optimization problem, the simulation obtains the reflection coefficient is slightly lower than that of the test, and the maximal error error is controlled at ±7.5dB around, and the two results are basically in agreement.

Keywords: Hilbert space, quantum approximation algorithm, Hamiltonian quantity, optical-microwave entanglement, OMA wave transmission in air

1. Introduction

Quantum entanglement is a core resource for quantum computing and quantum communication

✉ Corresponding author.
E-mail address: zhanghao1726@126.com (H. Zhang).
Received 15 September 2024; Revised 05 November 2024; Accepted 20 February 2025; Published Online 16 April 2025.
DOI: 10.61091/jcmcc127b-134

networks. As one of the most remarkable features of quantum mechanics, quantum entanglement has become an important resource in the field of quantum information processing [1-2]. So far, the preparation and manipulation of entangled states have been verified not only in microscopic systems but also in macroscopic systems. Various types of optical systems have been utilized in microscopic systems, such as four-wave mixing systems, optical parametric oscillators and optical parametric amplifiers to realize multi-component entanglement, as well as the preparation of large-scale entanglement [3-6]. And the cavity photo dynamics, which is formed by the nonlinear coupling of photons and mechanical oscillators through radiation pressure, provides a new way for the realization of macroscopic quantum entanglement and has made remarkable progress in theory and experiment, including the realization of entanglement between a mechanical oscillator and an electromagnetic field, entanglement between two mechanical oscillators, and quantum compression of mechanical motion [7-10].

Similar to the cavity optical force system, cavity magnetism has attracted great interest in macroscopic quantum effects. In the past decade, magneton-based composite architectures have promising applications in quantum information processing, quantum sensing, and quantum networks [11-12]. In particular, the coupling between magnons and microwave or optical photons opens up possibilities for optical control, design, detection, and transmission of magneton states, as well as obtaining quantum entanglement or guidance for the system when compressed light is utilized to drive cavity modes, among other richer properties [13-14].

Hybrid quantum systems composed of multiphysics systems can synthesize the advantages of different degrees of freedom and play an important role in the development of quantum technology [15]. In recent years, hybrid systems composed of cavity and magnetic systems have attracted attention [16]. The spin-wave quantized quasiparticles in the magnetic system are called magnetic vibrators, which have good tunability and can be coupled to microwaves through magnetic coupling interactions, to optical fields through magneto-optical effects, to phonons using magnetostrictive effects, and to superconducting quantum bits indirectly by means of microwave fields [17-19].

This property of magnetic vibrators makes hybrid quantum systems based on magnetic vibrators expected to be a platform for the development of novel quantum technologies [20]. In conventional information processing, the free charge of semiconductor devices is often utilized to transmit information, but when the processing unit is as small as the nanometer scale, problems such as Joule heating and uncontrollable ground quantum effects will inevitably occur, exacerbating the functional loss of the device [21-22]. Compared with relying on conduction electrons to transmit information, magnetic vibrators are electrically neutral, and information transmission by magnetic vibrators as carriers has the advantage of no heat loss, so the hybrid system based on magnetic vibrators has a promising application in magneton information transmission and magneton quantum devices [23-24].

In this paper, the full state of the system is expressed through an equation based on the tensor direct product of the Hilbert space. A quantum approximate optimization algorithm is proposed to compute the unit matrix using three 2×2 positive ergodic complex matrices to form the bubbleley operator. According to the adiabatic theorem, the workflow of the quantum approximate optimization algorithm is sorted out starting from the ground state of the Hamiltonian quantity, and the quadratic unconstrained binary optimization method is proposed to solve the constrained problem. The performance of the UQAOA algorithm is evaluated by dealing with the generalized operator form of the constrained mixed Hamiltonian quantities within a given QAOA framework. Construct a model of cavity magnetism, analyze the generation of electromagnetic waves in quantum entanglement, obtain the Langevin equation satisfied by the averaging field, and reason about the effective coupling strength of opto-magnetism enhanced by an external field drive. Based on the concept of quantum state and statistical state OAM electromagnetic wave, the quantum state transmission characteristics of electromagnetic wave are analyzed in combination with UQAOA algorithm.

2. Quantum entanglement

2.1. Entanglement-based effects

For a multiparty system containing n subsystem, its Hilbert space H is the tensor direct product of the subsystem spaces $H=\otimes_{l=1}^{n}H_l$. The principle of superposition of states permits to write the full state of the system in this form:

$$|\Phi\rangle=\sum_{i_1,\dots,i_n}c_{i_1,\cdots,i_n}\left|i_1\right\rangle\otimes\left|i_2\right\rangle\otimes\cdots\left|i_n\right\rangle \tag{1}$$

This state may not in general be written as a direct product state of independent subspaces $|\Phi\rangle\neq\left|\Phi_1\right\rangle\otimes\left|\Phi_2\right\rangle\otimes\cdots\otimes\left|\Phi_n\right\rangle$. This relation implies that it is not possible in a general sense to assign a monomorphic vector to any subsystem of the system. The resulting relation leads to the possibility of constructing superposition states of the finger order of magnitude with resources of linear magnitude.

For pure states, an entangled state is defined in such a way that its state cannot be written as a direct product state. For mixed states, entangled mixed states need to be redefined and are defined as convex combinations whose states cannot be written as straight product states:

$$\rho\neq\sum_i p_i\rho_1^i\otimes\ldots\otimes\rho_n^i \tag{2}$$

States that do not satisfy the above conditions are called differentiable states.

The Hilbert space of a bipartite state system $H=H_1\otimes H_2$ with dimension $\dim H_1=\dim H_2=2$. This system is unfolded by four Bell state entangled bases:

$$\left|\Psi^{\pm}\right\rangle=\frac{1}{\sqrt{2}}(|0\rangle|1\rangle\pm|1\rangle|0\rangle),\left|\Phi^{\pm}\right\rangle=\frac{1}{\sqrt{2}}(|0\rangle|0\rangle\pm|1\rangle|1\rangle) \tag{3}$$

This state is pure as a holomorphic state, and the projection to the subsystem is to obtain a mixed state with probability $1/2$ for the $|0\rangle$ -state and $|1\rangle$ -state, respectively. Moreover, this state maximally violates the Bell-CHSH inequality [25].

2.1.1. Quantum state transport. The unknown quantum state $|q\rangle=a|0\rangle+b|1\rangle$ of system A is transferred to Bob's side through the EPR state formed by system A' of his side together with system B of Bob's side. The state is represented as:

$$\left|\Psi_{AA'B}\right\rangle=|q\rangle_A\otimes\frac{1}{\sqrt{2}}[|0\rangle|0\rangle+|1\rangle|1\rangle]_{A'B} \tag{4}$$

Under the Bell state base, this state can be rewritten as:

$$\begin{aligned}\left|\Psi_{AA'B}\right\rangle=\frac{1}{2}\Big[&\Phi_{AA'}^{+}\left(a|0\rangle_B+b|1\rangle_B\right)+\Phi_{AA'}^{-}\left(a|0\rangle_B-b|1\rangle_B\right)\\&+\Psi_{+}^{AA'}\left(a|1\rangle_B+b|0\rangle_B\right)+\Psi_{AA'}^{-}\left(a|1\rangle_B-b|0\rangle_B\right)\Big]\end{aligned} \tag{5}$$

When Alice measures AA' under the Bell basis, corresponding to four different Bell states, the Bob-side system B collapses with equal probability to the corresponding four different states. Alice then informs Bob of her measurement via classical communication, and Bob can then implement the following four different Bubbleley transformations on her side's bits to obtain the initial state $|q\rangle$ that Alice wants to transmit:

$$\sigma_0 = \begin{pmatrix} 1 & 0 \\ 0 & 1 \end{pmatrix}, \sigma_1 = \begin{pmatrix} 1 & 0 \\ 0 & -1 \end{pmatrix} \tag{6}$$

$$\sigma_2 = \begin{pmatrix} 0 & 1 \\ 1 & 0 \end{pmatrix}, -i\sigma_3 = \begin{pmatrix} 0 & -1 \\ 1 & 0 \end{pmatrix} \tag{7}$$

2.1.2. Entanglement switching. In long-distance quantum communication or quantum cryptography, to realize the entanglement of matter at a distance, some scholars propose the method of entanglement exchange.

Alice and Clare share a maximally entangled state $\left|\Phi^+\right\rangle = \frac{1}{\sqrt{2}}[|0\rangle|0\rangle + |1\rangle|1\rangle]_{AC}$, and Bob and David share the same state, this quadratic state is:

$$|\Psi\rangle_{ACBD} = \left|\Phi^+\right\rangle_{AC} \otimes \left|\Phi^+\right\rangle_{BD} \tag{8}$$

Under Bell's base, a joint measurement is done on the bits of Clare and Bob. Clare and Bob inform Alice and David of the result, and Alice and David then do a local rotation transformation to obtain the entangled state $\left|\Phi^+\right\rangle_{AD}$. So, Alice and David can obtain the entangled state without going through direct contact.

2.2. Entanglement metric

2.2.1. Quantum approximation algorithm based on constrained optimization algorithm. Quantum Approximate Optimization Algorithm (QAOA) is a variable quantum algorithm designed to provide solutions to combinatorial optimization problems [26].

A Bubbleley operator is a set of three 2×2 of a muon positive ergodic complex matrix, which is generally denoted by the Greek letter σ, pronounced as Bubbleley x, Bubbleley y, Bubbleley z:

$$\sigma_x = \begin{bmatrix} 0 & 1 \\ 1 & 0 \end{bmatrix} \sigma_y = \begin{bmatrix} 0 & -i \\ i & 0 \end{bmatrix} \sigma_z = \begin{bmatrix} 1 & 0 \\ 0 & -1 \end{bmatrix} \tag{9}$$

Each bubbleley matrix has two eigenvalues, +1 and -1, whose corresponding normalized eigenvectors are:

$$\begin{aligned} \psi_{x+} &= \frac{1}{\sqrt{2}}\begin{bmatrix} 1 \\ 1 \end{bmatrix} \psi_{y+} = \frac{1}{\sqrt{2}}\begin{bmatrix} 1 \\ i \end{bmatrix} \psi_{z+} = \begin{bmatrix} 1 \\ 0 \end{bmatrix} \\ \psi_{x-} &= \frac{1}{\sqrt{2}}\begin{bmatrix} 1 \\ -1 \end{bmatrix} \psi_{y-} = \frac{1}{\sqrt{2}}\begin{bmatrix} 1 \\ -i \end{bmatrix} \psi_{z-} = \begin{bmatrix} 0 \\ 1 \end{bmatrix} \end{aligned} \tag{10}$$

Typically, $|+\rangle$ is used to represent ψ_{x+}, $|-\rangle$ is used to represent ψ_{x-}, $|0\rangle$ is used to represent ψ_{z+}, and $|1\rangle$ is used to represent ψ_{z-}.

The corresponding arithmetic rules for bubbly operators are as follows; multiplying the same bubbly operator gives the unit matrix. Bubble x multiplied by bubble y equals i times bubble z. Bubble y multiplied by bubble x equals $-i$ times bubble z.

2.2.2. Workflow of the quantum approximation optimization algorithm：

1) Adiabatic Quantum Computing. Adiabatic quantum computation is the solution of specific problems and other combinatorial search problems by the following process. Usually such a problem is to find a state satisfying $C_1 \wedge C_2 \wedge \cdots \wedge C_M$ that the expression contains M subproblems that can satisfy the condition, each of which C_i has a value of True or False and may contain n bits, where each bit is a variable $x_j \in \{0,1\}$ so that C_i it is a Boolean-valued function with respect to $x_1, x_2, \cdots, x_n$ The adiabatic quantum algorithm solves this type of problem using quantum adiabatic

evolution. It starts with an initial Hamiltonian quantity H_B:

$$H_B = H_{B_1} + H_{B_2} + \cdots + H_{B_M} \tag{11}$$

Here H_{B_i} corresponds to the Hamiltonian of that subproblem C_i, and the usual choice of H_{B_i} does not depend on other subproblems. It then undergoes an adiabatic evolution ending with the Hamiltonian quantity H_p of the problem:

$$H_p = \sum_C H_{P,C} \tag{12}$$

Here $H_{P,C}$ is a Hamiltonian quantity that satisfies Problem C, which has eigenvalues 0 and 1. If Subproblem C satisfies the condition, the eigenvalue is 1, and if it does not, the eigenvalue is 0. For a simple adiabatic evolutionary path such as:

$$H(t) = \left(1 - \frac{t}{T}\right) H_B + \frac{t}{T} H_P \tag{13}$$

Let $\mathrm{s} = \frac{t}{T}$, then there is:

$$\tilde{H}(t) = (1-s) H_B + (s) H_P \tag{14}$$

This is the adiabatic evolution of the Hamiltonian quantity of the algorithm.

According to the adiabatic theorem, starting from the ground state of the Hamiltonian H_B and, first, going through an adiabatic process, ending H_p with the ground state of the Hamiltonian of the problem, and then measuring the final state n of the spin's z components, which will produce a string $Z_1, Z_2, \cdots, Z_n$ which is likely to be the result of the problem.

2) Quantum approximation optimization algorithm. The quantum approximate optimization algorithm provides an idea for designing parametric quantum circuits for combinatorial optimization problems. The quantum approximation optimization algorithm is inspired by the adiabatic theorem to construct parameterized quantum circuits similar to the adiabatic evolution to solve the base state of the problem Hamiltonian quantity. This evolution is shown in Fig. 1. Where $|s\rangle$ is the initial quantum state of the evolution, $\hat{B}$ is called the hybrid Hamiltonian, which corresponds to the initial Hamiltonian in the adiabatic evolution H_B, and induces the operator with covariates $e^{-i\beta\hat{B}}$, and $\hat{C}$ is called the problem Hamiltonian, which corresponds to the terminating Hamiltonian in the adiabatic evolution H_p, and induces the operator with covariates $e^{-i\gamma\hat{c}}$. The system undergoes p iterations and adjusts the values of β and γ at each step of evolution, and the system eventually converges to a certain base state of the problem Hamiltonian $\hat{C}$ with a high probability. Hamiltonian 11. This ground state corresponds to the solution of the problem. This evolution process can be expressed as the following parametric transformation:

$$|\left|\vec{\beta}, \vec{\gamma}\right\rangle = e^{-i\beta_p \hat{B}} e^{-i\gamma_p \hat{C}} \ldots e^{-i\beta_1 \hat{B}^B} e^{-i\gamma_1 \hat{c}_1} |s\rangle \tag{15}$$

where β_i, $\gamma_i \in [-\pi, \pi]$, $\vec{\beta} = (\beta_1, \beta_2, \ldots, \beta_p)$, $\vec{\gamma} = (\gamma_1, \gamma_2, \ldots, \gamma_p)$. $\vec{\beta}$, $\vec{\gamma}$ are parameters that can be optimized and p is the number of iterations.

The parameters $\vec{\beta}$, $\vec{\gamma}$ are optimized using the classical optimizer, and the expectation value of $\hat{C}$ on $|\psi(\vec{\beta}, \vec{\gamma})\rangle$ is obtained by making measurements on the quantum state $|\psi(\vec{\beta}, \vec{\gamma})\rangle$:

$$f(\vec{\beta}, \vec{\gamma}) = \langle \psi(\vec{\beta}, \vec{\gamma}) | \hat{C} | \psi(\vec{\beta}, \vec{\gamma}) \rangle \tag{16}$$

The obtained expectation $f(\vec{\beta}, \vec{\gamma})$ is the optimal solution of the combinatorial optimization problem.

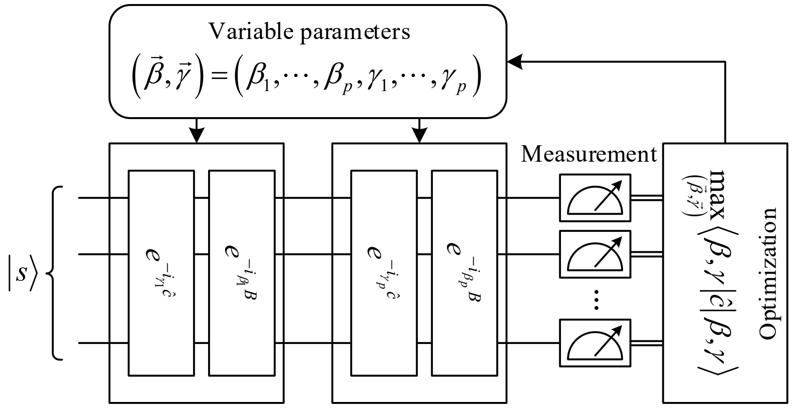

Fig. 1. QAOA Work flow

2.2.3. Methods for solving constrained problems：

1) Quadratic unconstrained binary optimization methods. Quadratic unconstrained binary optimization methods, which are improved algorithms to quantum approximate optimization algorithms, are now widely studied and used to model and solve many classes of optimization problems. The objective of a constrained optimization problem is to minimize or maximize a cost function that can be physically interpreted as finding the ground state of a typical Ising Hamiltonian function. The quadratic unconstrained binary optimization method improves the quality of the solution and the running time by converting the constraints of the problem into a cost function through preprocessing. A major advantage of quadratic unconstrained binary optimization is that it provides a unified algorithmic framework suitable for solving many types of problems.

When dealing with optimization problems with constraints, the quadratic unconstrained binary optimization method makes it possible to obtain the exact expectation faster in the framework of quantum approximation optimization algorithms by adding a penalty term to the Hamiltonian quantity $\hat{C}$, which will be worse than the solution that meets the expectation of the problem. Taking the classical approach to the maximum independent set problem as an example, the initial quantum state $|s\rangle=\Sigma_{x=0}^{2^n-1}|x\rangle$, is the full set that contains both feasible and infeasible solutions. The mixed Hamiltonian quantity $B=\sum_i \sigma_i^x$, called the transverse field operator, is the sum of the bubbleley X operator acting on each quantum bit i. The problem Hamiltonian $\hat{C}$ is shown in equation (17) [27]:

$$\hat{C}=\sum_{x=0}^{2^n-1}\vec{x}\cdot\vec{e}\,|x\rangle\langle x|-\sum_{(i,j)\in E}\frac{\sigma_i^z-1}{2}\frac{\sigma_j^\chi-1}{2} \tag{17}$$

where $\vec{e}=(11\ldots1)^T$, with a penalty term of $\sum_{(i,j)\in E}\frac{\sigma_T^*-1}{2}\frac{\sigma_j^*-1}{2}$, ensures that the value of the corresponding solution (infeasible solution) is less than the feasible solution when there is an edge connected between i and j.

2) Quantum alternating operator fitting method. Different basis states are set instead of a fixed initial basis state according to different problems, and the full set of uniform superposition states is transformed into the feasible solution uniform superposition states, and the essence of this extension is known as the quantum alternating operator fitting method. For the case where mixing is only required in the desired subspace, initial Hamiltonian quantities run mixed on the feasible solution subspace ground state can yield more efficient results than in the original framework. This approach is particularly useful for optimization problems with constraints, where the set of satisfied constraints is defined as a feasible solution subspace. It makes it more efficient to obtain good results for the problem in the framework of quantum approximate optimization algorithms.

When dealing with problems with constraints, the initial quantum state of the quantum alternating operator fitting method contains only the feasible solution evolution space, i.e., the set of all solutions satisfying the constraints in the solved optimization problem with constraints. The hybrid Hamiltonian $\hat{B}$ restricts the evolution of the quantum state to the space of feasible solutions of the constrained optimization problem Ω, given the initial state in the partial hybrid Hamiltonian as shown in Eq. (18):

$$|s\rangle = \sum_{\vec{x}\in\Omega} |x\rangle \tag{18}$$

The Hamiltonian quantity $\hat{B}$ is shown in Eq. (19) and is mixed only in the initial state $|s\rangle$:

$$\hat{B} = \sum_{j=1}^{n} 2^{-D_j} \sigma_i^x \prod_{i\in nbhd(j)} \left(I - \sigma_i^z\right) \tag{19}$$

where j is a vertex of the graph, D_j is the degree of vertex j, and $nbhd(j)$ is a neighboring vertex of j.

2.2.4. Performance analysis. In subsection 2.2.3, a generalized operator form and a unified algorithmic flow for handling hybrid Hamiltonian quantities with these constraints within the QAOA framework is given and referred to as UQAOA.In this section, the performance of the UQAOA algorithm is evaluated by means of its performance on the Graph Partition problem. On the Graph Partition problem, the UQAOA algorithm is compared with the standard QAOA, the cyclic XY algorithm, and the complete graph XY algorithm on 10 randomly generated graphs, and Fig. 2 shows a comparison of the approximation ratios of several algorithms for solving the Graph Partition problem.

Figure 2 shows the approximation ratios of different algorithms as p increases. High approximation ratios are achieved faster with smaller p, whereas standard QAOA based has the problem of reachability defects. After p reaches a certain value p*, no better approximation ratio can be achieved by increasing p. In the Graph Partition problem, the UQAOA algorithm achieves comparable performance to the full graph XY algorithm and a large improvement over the cyclic XY algorithm, keeping the approximation ratio around 1 after the number of levels p = 4.

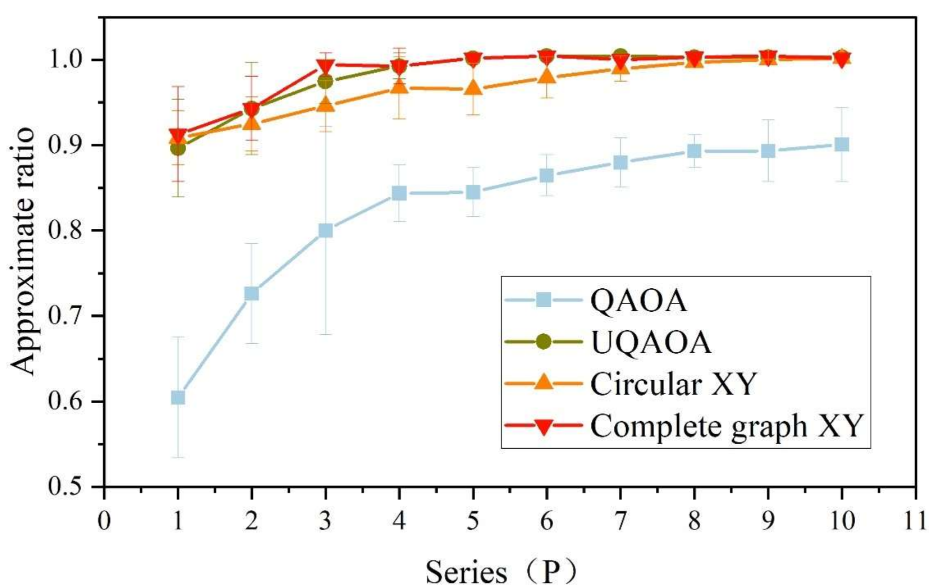

Fig. 2. Several algorithms for the problem of graph partition are approximated

Figure 3 shows a comparison of the running times of several algorithms for solving the Graph

Partition problem, with (a) for P = 2 and (b) for P = 5, recorded for each algorithm on the simulator for 10 random graphs. The times include finding the optimal parameters using the classical strategy β and γ. The scatter plots show that the UQAOA algorithm converges faster compared to the cyclic XY algorithm and the complete graph XY algorithm. The UQAOA algorithm completed convergence in a running time of 3.145s when P = 2 and 40.345 when P = 5. However, many factors need to be taken into account when performing real-time performance tests in an environment where quantum algorithms are actually applied, such as infrastructure (if the QAOA implementation is on a local computer connected to a remote quantum computer, the communication time should be recorded). In the future, runtime performance should be rigorously evaluated when appropriate conditions are available.

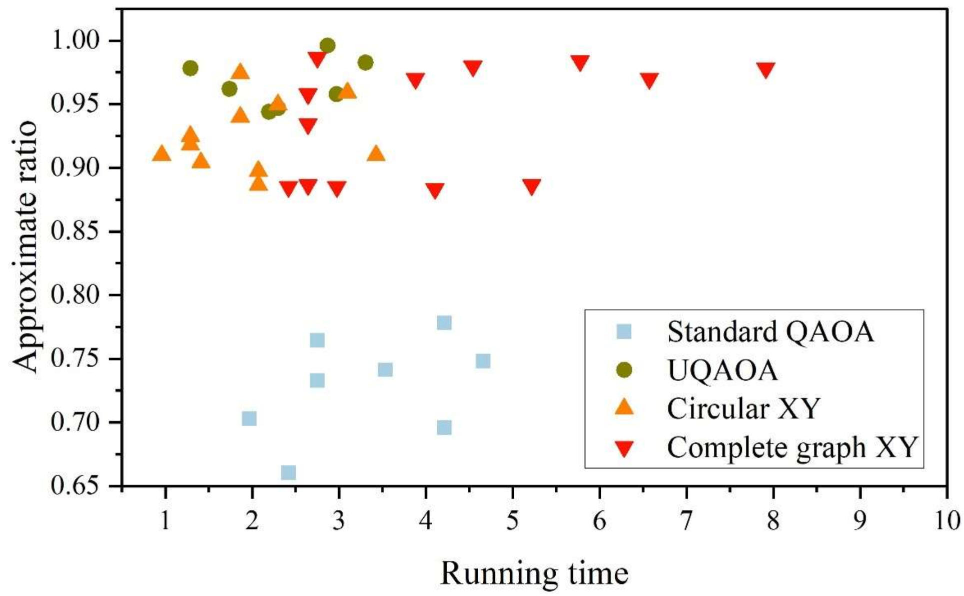

(a)P=2

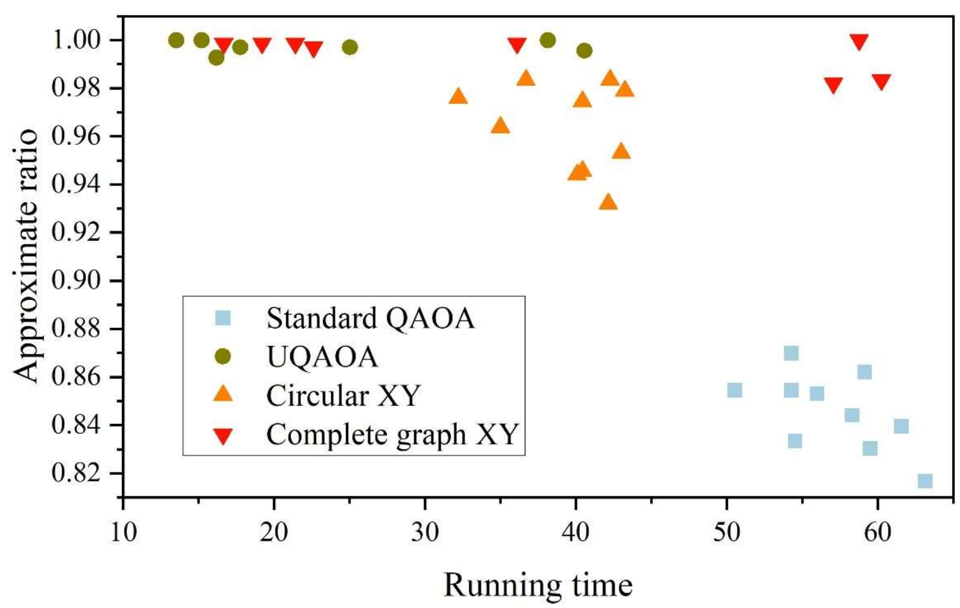

(b)P=5

Fig. 3. Several algorithms for the problem of graph partition are compared

3. Generation of electromagnetic waves in quantum entanglement

3.1. Theory of Cavity Magnetism

Quasiparticles with quantized spin waves in the magnetic system are called magnetic vibrators, which have good tunability and can be coupled to microwaves through magnetic coupling interactions, to optical fields through magneto-optical effects, to phonons using magnetostrictive effects, and to superconducting quantum bits indirectly with the help of microwave fields [28]. This property of magnetic vibrators makes hybrid quantum systems based on magnetic vibrators expected to be a platform for the development of novel quantum technologies. In conventional information processing, the free charge of semiconductor devices is often utilized to transmit information, but when the processing unit is as small as the nanometer scale, problems such as Joule heating and uncontrollable quantum effects will inevitably occur, exacerbating the functional loss of the device.

3.2. Models and Hamiltonian quantities

Figure 4(a) shows a schematic diagram of the system. A YIG sphere is placed in the microwave cavity, in which the TE echo wall modes are coupled with the light passing through the nanofiber. Fig. 4(b) shows a schematic diagram of the coupling relationship of each mode. The magnetic vibrator mode m is coupled to the optical modes a_1 and a_2 through the magneto-optical effect and to the microwave mode b through the magnetic dipole interaction. The magnetic vibrator mode acts as a cooling reservoir to enhance the microwave-optical wave entanglement.

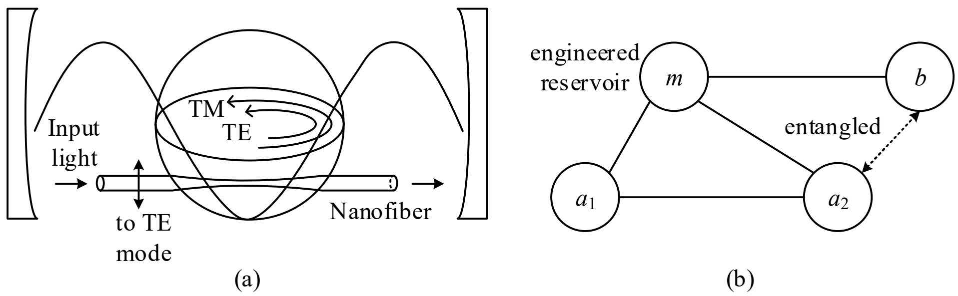

Fig. 4. Models and Hamiltonian quantities

As shown in Fig. 4, a magnetic vibrator mode, a microwave cavity mode and two echo-wall optical modes are included in the considered hybrid quantum system. The magnetic vibrator mode interacts with the two optical modes through the magneto-optical effect and couples to the microwave cavity mode through the magnetic dipole interaction. The two optical modes are confined near the equator of the YIG sphere and are defined as the transverse magnetic mode (TM) and the transverse electric mode (TE). In this paper, only the TE mode is driven by an external field. Based on the Hamiltonian quantities given in Chapter 2 for the opto-magnetic coupling as well as for the coupling of the magnetic oscillator to the microwave cavity, the total Hamiltonian of the system is:

$$\begin{aligned} H &= \omega_1 a_1^\dagger a_1 + \omega_2 a_2^\dagger a_2 + \omega_m m^\dagger m + \omega_b b^\dagger b + g\left(a_1^\dagger a_2 m + a_1 a_2^\dagger m^\dagger\right) \\ &+ G_{mb}\left(b^\dagger + b\right)\left(m^\dagger + m\right) + \Omega\left(a_1 e^{i\omega_2 t} + a_1^\dagger e^{-i\omega_2 t}\right) \end{aligned} \tag{20}$$

where a_1, a_2, m, and b are annihilation operators for TE mode, TM mode, magnetic vibrator mode, and microwave cavity mode, corresponding to frequencies ω_1, ω_2, ω_m, and ω_b, respectively.The term $g\left(a_1^\dagger a_2 m + a_1 a_2^\dagger m^\dagger\right)$ in the Hamiltonian quantity represents two optical modes coupled to a magnetic vibrator with a coupling strength of g, g which can reach a maximum at triple resonance conditions, i.e., at $\omega_1 = \omega_2 + \omega_m$. This term represents the annihilation of a a_1-mode photon accompanied by the production of a a_2-mode photon and a magnetic oscillator. The coupling term $G_{mb}\left(b^\dagger + b\right)\left(m^\dagger + m\right)$ indicates that the magnetic vibrator interacts with the microwave cavity with a G_{mb} coupling strength. Setting the dissipation of the microwave cavity mode and the magnetic oscillator mode as κ_b and κ_m, the microwave cavity-magnetic oscillator coupling term can be transformed to $G_{mb}\left(mb^\dagger + m^\dagger b\right)$ by the spin-wave approximation when the conditions of ω_m, $\omega_b \gg G_{mb}$, κ_b, and κ_m are satisfied. The last term in Eq. (20) represents the driving term with an external field frequency of ω_L and an amplitude of Ω. Under the representation rotating at the driving field frequency, the system Hamiltonian quantity can be written as:

$$\begin{aligned} H_s &= \Delta_a a_2^\dagger a_2 + \omega_m m^\dagger m + \omega_b b^\dagger b + g\left(a_1^\dagger a_2 m + a_1 a_2^\dagger m^\dagger\right) \\ &+ G_{mb}\left(mb^\dagger + m^\dagger b\right) + \Omega\left(a_1 + a_1^\dagger\right) \end{aligned} \tag{21}$$

where $\Delta_a = \omega_2 - \omega_L = -\omega_m$. The system is described by the following Lanzmann equation:

$$\begin{aligned}
\dot{a}_1 &= -i\left(g a_2 m + \Omega\right) - \frac{\kappa_1}{2} a_1 + \sqrt{\kappa_1} a_{1,in} \\
\dot{a}_2 &= -i\left(\Delta_a a_2 + g a_1 m^{\dagger}\right) - \frac{\kappa_a}{2} a_2 + \sqrt{\kappa_a} a_{2,in} \\
\dot{m} &= -i\left(\omega_m m + g a_1 a_2^{\dagger} + G_{mb} b\right) - \frac{\kappa_m}{2} m + \sqrt{\kappa_m} m_{in} \\
\dot{b} &= -i\left(\omega_b b + G_{mb} m\right) - \frac{\kappa_b}{2} b + \sqrt{\kappa_b} b_{in}
\end{aligned} \tag{22}$$

where κ_1 and κ_a are the dissipation of TE and TM modes, respectively, and $O_{in}\left(O = a_1, a_2, m, b\right)$ is the zero-mean input noise operator of the corresponding mode, satisfying the following correlation function:

$$\left\langle O_{in}(t) O_{in}^{\dagger}(t')\right\rangle = \left(N_o + 1\right)\delta\left(t - t'\right) \tag{23}$$

$$\left\langle O_{in}^{+}(t) O_{in}(t')\right\rangle = N_o \delta\left(t - t'\right) \tag{24}$$

where $N_O = \left[\exp\left(\hbar\omega_L / k_B T\right) - 1\right]^{-1}$ is the average thermal state Buchu number for the corresponding mode, where k_B is the Boltzmann constant, and T is the ambient temperature. This can be obtained by decomposing the operator into averaging and rising and falling terms: $a_1 \to a_1 + \alpha_1$, $a_2 \to a_2 + \alpha_2$, $m \to m + \beta$, $b \to b + \gamma$. Substituting them into Eq. (22) yields the Langevin equation satisfied by the averaging site:

$$\begin{aligned}
\dot{\alpha}_1 &= -i\left(g\alpha_2\beta + \Omega\right) - \frac{\kappa_1}{2}\alpha_1 \\
\dot{\alpha}_2 &= -i\left(\Delta_a\alpha_2 + g\alpha_1\beta^{*}\right) - \frac{\kappa_a}{2}\alpha_2 \\
\dot{\beta} &= -i\left(\omega_m\beta + g\alpha_1\alpha_2^{*} + G_{mb}\gamma\right) - \frac{\kappa_m}{2}\beta \\
\dot{\gamma} &= -i\omega_b\gamma - iG_{mb}\beta - \frac{\kappa_b}{2}B
\end{aligned} \tag{25}$$

Let the initial give β mode one translation $ig\alpha_1\alpha_2^{*} + iG_m\gamma$, and in steady state $\dot{\beta} = 0$, it can be obtained as $\beta = 0$. The other average amplitudes are obtained as $\alpha_1 = -\frac{2i\Omega}{\kappa_1}$, $\alpha_2 = 0$, and $\gamma = 0$.

After neglecting the terms of higher order minima, the Ronzwan equation describing the rise and fall of the system is as follows:

$$\begin{aligned}
\dot{a}_1 &= -\frac{\kappa_1}{2} a_1 + \sqrt{\kappa_1} a_{1,in} \\
\dot{a}_2 &= -i\left(\Delta_a a_2 + G_{ma} m^{\dagger}\right) - \frac{\kappa_2}{2} a_2 + \sqrt{\kappa_a} a_{2,in} \\
\dot{m} &= -i\left(\omega_m m + G_{ma} a_2^{\dagger} + G_{mb} b\right) - \frac{\kappa_m}{2} m + \sqrt{\kappa_m} m_{in} \\
\dot{b} &= -i\left(\omega_b b + G_{mb} m\right) - \frac{\kappa_b}{2} b + \sqrt{\kappa_b} b_{in}
\end{aligned} \tag{26}$$

where $G_{ma} = g\alpha_1$ is the optomagnetic effective coupling strength that can be enhanced by an external field drive.

Let $a_2 \to a_2 e^{-i\Delta_a t}$, $m \to m e^{-i\omega_m t}$, $b \to b e^{-i\omega_b t}$.

$$\begin{aligned} \dot{a}_2 e^{-i\Delta_a t} - i\Delta_a a_2 e^{-i\Delta_a t} &= -i\left(\Delta_a a_2 e^{-i\Delta_i t} + G_{ma} m^\dagger e^{i\omega_a t}\right) \\ &\quad -\frac{\kappa_2}{2} a_2 e^{-i\Delta_a t} + \sqrt{\kappa_a} a_{2in} \\ \dot{m} e^{-i\omega_\infty t} - i\omega_m m e^{-i\omega_\omega t} &= -i\left(\omega_m m e^{-i\omega_\infty t} + G_{ma} a_2^\dagger e^{i\Lambda_n t} + G_{mb} b e^{-i\omega_\infty t}\right) \\ &\quad -\frac{\kappa_m}{2} m e^{-i\omega_\infty t} + \sqrt{\kappa_m} m_{in} \\ \dot{b} e^{-i\omega_\mu t} - i\omega_b b e^{-i\omega_a t} &= -i\left(\omega_b b e^{-i\omega_n t} + G_{mb} m e^{-i\omega_\alpha t}\right) \\ &\quad -\frac{\kappa_b}{2} b e^{-i\omega_n t} + \sqrt{\kappa_b} b_{in} \end{aligned} \tag{27}$$

Organize to get:

$$\begin{aligned} \dot{a}_2 &= -iG_{ma} m^\dagger - \frac{\kappa_2}{2} a_2 + \sqrt{\kappa_a} a_{2,in} \\ \dot{m} &= -i\left(G_{ma} a_2^\dagger + G_{mb} b\right) - \frac{\kappa_m}{2} m + \sqrt{\kappa_m} m_{in} \\ \dot{b} &= -iG_{mb} m - \frac{\kappa_b}{2} b + \sqrt{\kappa_b} b_{in}, \end{aligned} \tag{28}$$

This yields the linearized Hamiltonian quantity in the interaction plotted view as:

$$H = G_{ma}\left(a_2 m + a_2^\dagger m^\dagger\right) + G_{mb}\left(m b^\dagger + m^\dagger b\right) \tag{29}$$

The first term of the Hamiltonian quantity of Eq. (29) is presented as a two-mode compressive interaction that can be used to entangle the optical mode a_2 and the magnetic oscillator mode m, and the second term describes a beamsplitter-type interaction that causes the magnetic oscillator mode m to exchange with the microwave mode b. The optical mode a_2 and the microwave mode b become entangled when both interactions occur simultaneously. To facilitate the description of microwave-optical entanglement, the Bogoliubov operator is introduced:

$$\begin{aligned} \beta_1 &= a_2 \cosh r + m^\dagger \sinh r \equiv S(r) a_2 S^\dagger(r) \\ \beta_2 &= m \cosh r + a_2^\dagger \sinh r \equiv S(r) b S^\dagger(r) \end{aligned} \tag{30}$$

where the compression parameter $r = \tanh^{-1}\left(G_{ma}/G_{mb}\right)$, the bimodal compression operator $S(r) = \exp\left[r\left(a_2 m - a_2^\dagger m^\dagger\right)\right]$. By applying the Bogoliubov operator, Eq. (29) can be rewritten as [29]:

$$H_{\text{int}} = \tilde{G}\beta_2 m^\dagger + H.c. \tag{31}$$

where $\tilde{G} = \sqrt{G_{mb}^2 - G_{ma}^2}$ is the effective coupling strength between the magnetic oscillator mode m and mode β_2. It is clear that modes m and β_2 are coupled via beam splitter type interactions, while mode β is not involved in the interaction with mode m, which is referred to as the dark mode. Using beamsplitter-type interactions, magnetic oscillator modes can be used to cool mode β_2. The ground state of Bogoliubov modes β_1 & β_2 corresponds to the two-mode compression state $|\psi\rangle = S(r)|0,0\rangle$, where $|0,0\rangle$ is the vacuum state of modes a_2 & b. This suggests that when the Bogoliubov mode is cooled to the ground state, the optical and microwave modes a_2 and b will be in the two-mode compressed state. Although the mode β_1 cannot be cooled through beamsplitter-type interactions, the researcher's work indicates that cooling the mode β_2 to the ground state is capable of producing sufficiently large optical-microwave entanglement.

3.3. Analysis of quantum entanglement variations

3.3.1. Variation of the compression parameter r during quantum entanglement. Fig. 5 shows the effect of the compression parameter r on the two-body entanglement in the system, and the light-microwave entanglement E_{ac} is first enhanced and then weakened with the increase of r, and there is an optimal value of r near 0.234. Since the entanglement of light and microwave is also an important resource for realizing quantum computation and so on, combined with the optimal path calculation of quantum entanglement of UQAOA algorithm, r=0.2 is taken in the calculation of results in this paper.

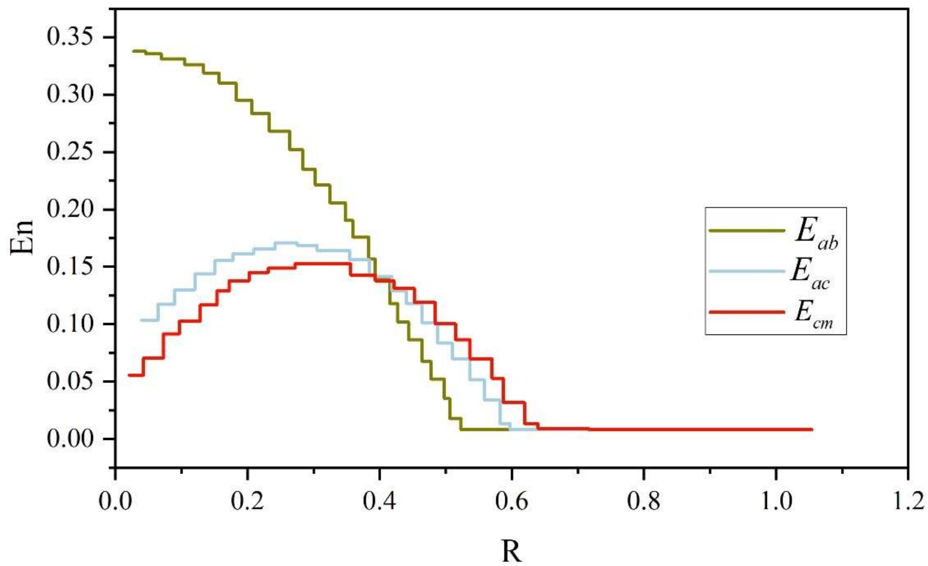

Fig. 5. The effect of compression parameter r on the two bodies in the system

3.3.2. Variation of effective coupling strength during quantum entanglement. The system coupling strength is very important for the generation of entangled states. Fig. 6 shows the trends of microwave-phonon and optical-magnetic entanglements E_{ab} and E_{cm} with magnetic coupling strength G_m, optical coupling strength G_c, and magnetic dipole interaction strength G_{am} between microwave-magnets, respectively. Fig. 6(a) shows the effective photodynamic coupling strength G_c, and the quantum entanglement E_{ab} and E_{cm} increases and then decreases with the enhancement of G_m. The quantum entanglement is shown in Fig. 6(b). E_{ab} It reaches the highest value of 0.436 at G_m 3.4. The reason is that with G_m enhancement, in addition to its own microwave-optical entanglement source E_{ac}, the entanglement generated by magnetostriction increases, which is transferred to the microwave force and magnetophoton system through the microwave-magneton state-exchange interactions as well as the action of the photoforce beamsplitter, and thus the entanglement E_{ab} and E_{cm} increases with G_m within a certain parameter range. However, as G_m continues to enhance, most of the magnons interact with the phonons, affecting the entanglement transfer, which results in the entanglement E_{cm} & E_{ab} starting to decrease. Fig. 6(b) shows the effective magnetic coupling strength G_m, and the entanglement E_{ab} & E_{cm} increases and then decreases as G_c becomes larger. E_{cm} reaches a maximum value of 0.155 at G_c 1. The reason for this is that at first the entanglement generated by time-microwave and magnetostriction is transferred to the microwave mechanics and magneto-photonic system through the microwave-magneton state-exchange interactions as well as the optical beam-splitter interactions, so that the entanglement E_{ab} vs. E_{cm} increases with the enhancement of G_c within a certain parameter range. However, when G_c continues to be enhanced, the optical photons interact with phonons as much as possible, which leads to a decrease in the entanglement source, which in turn leads to entanglement E_{cm} & E_{ab} starting to decrease. Fig. 6(c) shows the microwave-magneton coupling strength G_{am} and it is found that with G_{am} enhancement, the entanglement E_{ab} and E_{cm} change in the same trend, both of which first decrease to 0 with G_{am} enhancement, and then increase and then decrease with G_{am} enhancement. E_{ab} reaches a peak of 0.284 at G_{am} =3.48. The reason is that the microwave-magneton state-exchange interaction competes with the optical beamsplitter action at the beginning, but does not play a role in transferring the entanglement, and thus the entanglement E_{ab} and E_{cm} decreases first until it is zero. Afterwards, as G_{am} continues to get larger, the microwave-magneton state exchange interaction as well as the optical force beam splitter interaction begin to shift the two sources of entanglement, which results in entanglement E_{ab} and E_{cm} beginning to increase. But as G_{am} continues to intensify, most of the microwave photons interact with the magnets, resulting in fewer microwave photons interacting with optical photons as well as fewer magnets interacting with phonons, i.e., fewer sources of entanglement E_{ac} and E_{cm}, which in turn results in entanglement E_{ab} and E_{cm} beginning to decrease again. In contrast to the system in which microwaves and light themselves are not entangled, the entanglements E_{ab} and E_{cm} generated in the system in this paper can exist either simultaneously or separately. In particular, entanglement E_{ab} and E_{cm} still exist when G_{am} =0.

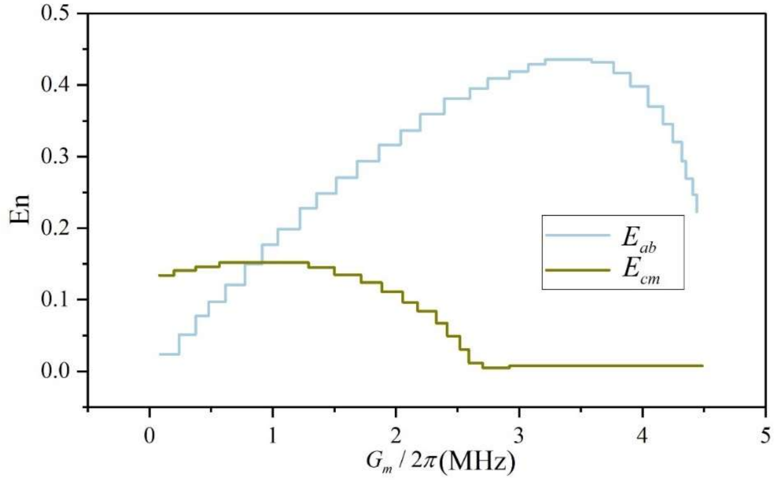

(a)Effective magnetic coupling strength G_m

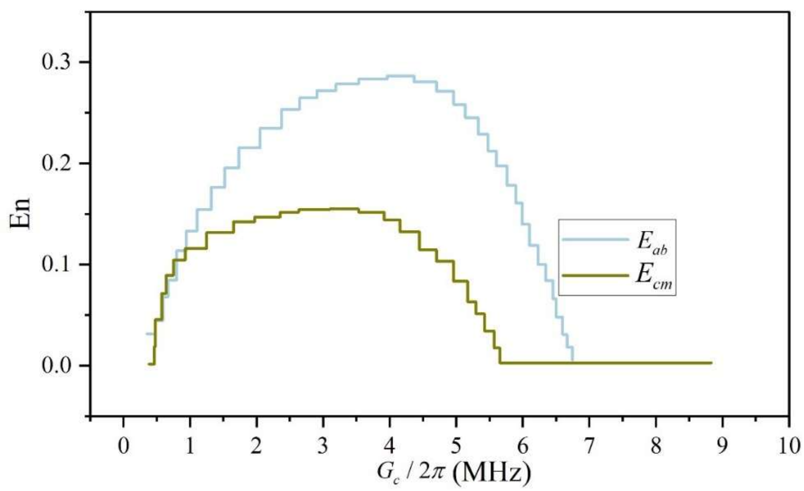

(b)Effective optical coupling intensity G_c

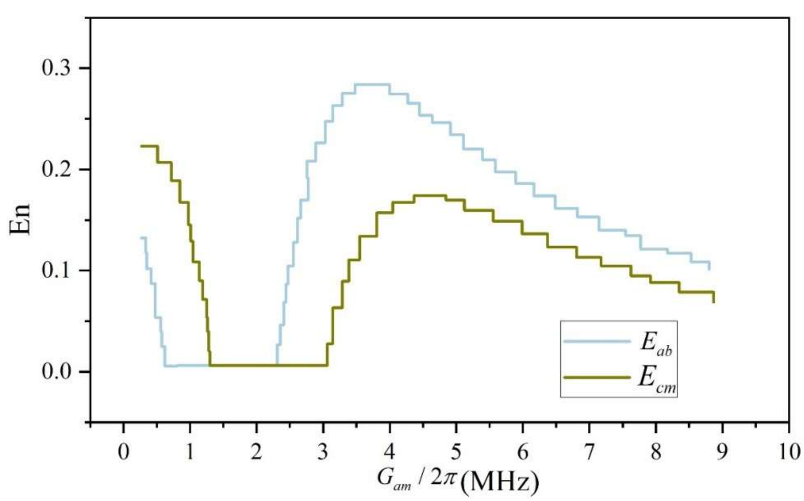

(c)Microwave-magneton coupling intensity G_{am}

Fig. 6. Changing trends

4. Analysis of the role of constraint-based optimization algorithms for quantum state transport

4.1. Quantum States and Electromagnetic Wave Transmission

4.1.1. Conceptual connotations of quantum state OAM electromagnetic waves. The angular momentum carried by an electromagnetic wave is divided into spin angular momentum and orbital angular momentum and can be expressed as:

$$J = L + S \tag{32}$$

Where: J is the total angular momentum, L is the orbital angular momentum, and S is the spin angular momentum, which characterizes the polarization of the electromagnetic wave, and according to the theory of electrodynamics, it can be computationally deduced to obtain the OAM that the electromagnetic wave has as:

$$\begin{aligned} L &= \frac{1}{\mu_0 c^2}\int_V r \times (E \times B) dv - S \\ &= \varepsilon_0 \int_V \sum_{i=1}^{3} E_i (r \times \nabla) A_i dv + \varepsilon_0 \int_V E \times A dv - S \\ &= \varepsilon_0 \int_V \sum_{i=1}^{3} E_i \left[\left(r^{(0)} + r^{(i)} \right) \times \nabla \right] A_i dv + \varepsilon_0 \int_V E \times A dv - S \\ &= L^{(e)} + L^{(i)} \end{aligned} \tag{33}$$

Where: μ_0 is the vacuum permeability, ε_0 is the vacuum permittivity, c represents the vacuum speed of light, r is the space coordinates, E is the electric field strength, B represents the magnetic induction strength, A is the magnetic vector potential, V is the integral space (the space in which the electromagnetic wave exists), dv is the space microelement, $r^{(e)}$ and $r^{(i)}$ are the distance vector from the origin of the internal orbital origin of the quantum of the electromagnetic wave to the reference coordinate system, and from any point of the space to the internal orbital origin, respectively. The sum of the two is the total position vector.

From Eq. (33), we can see that the OAM of the electromagnetic wave is related to its integration space, electric field strength and magnetic field strength.

4.1.2. UQAOA-based quantum state transmission properties of electromagnetic waves. Firstly, this chapter starts with the design of a rectangular antenna unit operating at 3.7 GHz, a circular patch antenna capable of generating +1 mode vortex electromagnetic waves, and the transmission characteristics of the generated OMA waves in air and the transmission optimization problem are analyzed based on the UQAOA algorithm. The circular patch is processed and tested, and Fig. 7 shows the reflection coefficients of the circular patch simulated and tested, Fig. (a) shows the upper patch and Fig. (b) shows the lower feed network.

After the test to get the reflection coefficient of the two ports from the figure can be seen, due to the loss of the dielectric substrate in the actual processing, the reflection coefficient obtained from the simulation is slightly lower than the test, the maximum error error control in ± 7.5dB or so, but the two results basically coincide.

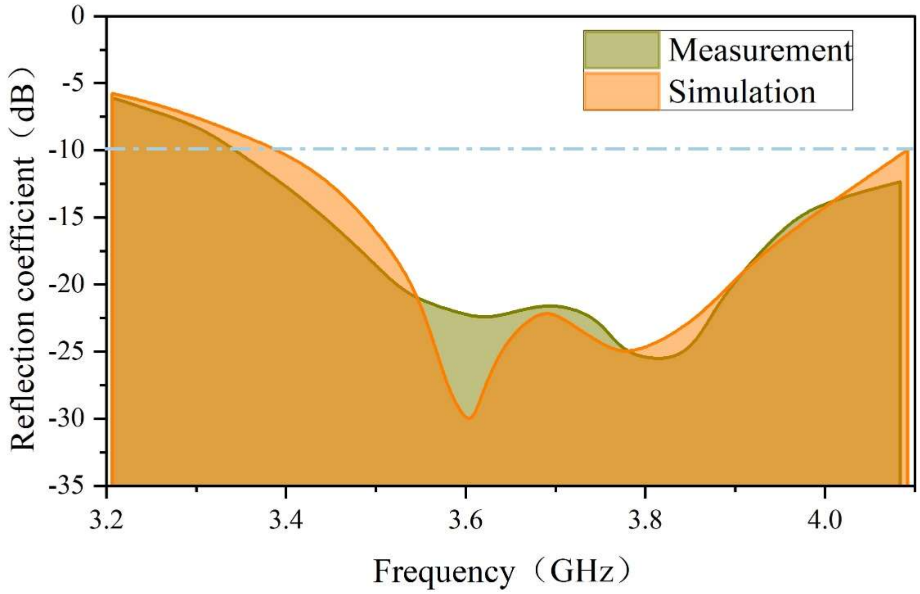

(a)Upper patch

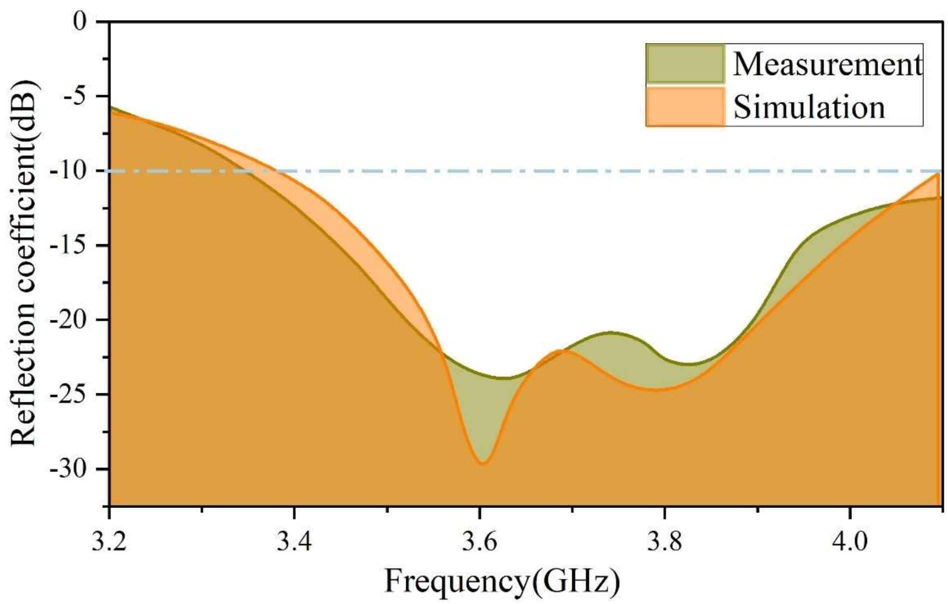

(b)Lower level feed network

Fig. 7. Circular patch simulation and test reflection coefficient

Fig. 8 shows the circular patch test orientation diagram, Fig. (a) shows the upper patch and Fig. (b) shows the lower feed network. From the figure, it can be seen that the gain of the antenna test decreases compared to the simulation results, but the error is within the acceptable range, especially in the lower feed network, the maximum error is about ±2.5.

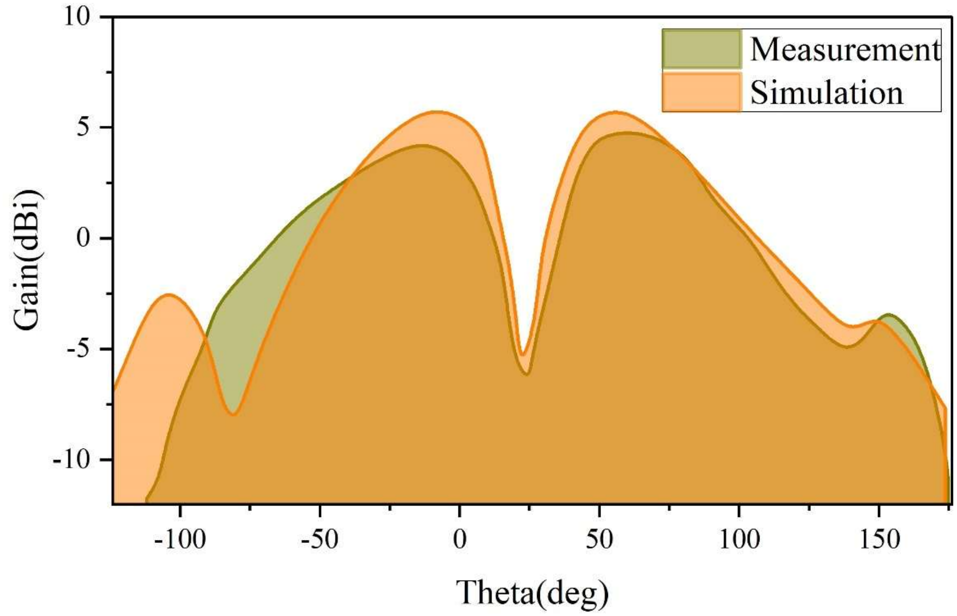

(a)Upper patch

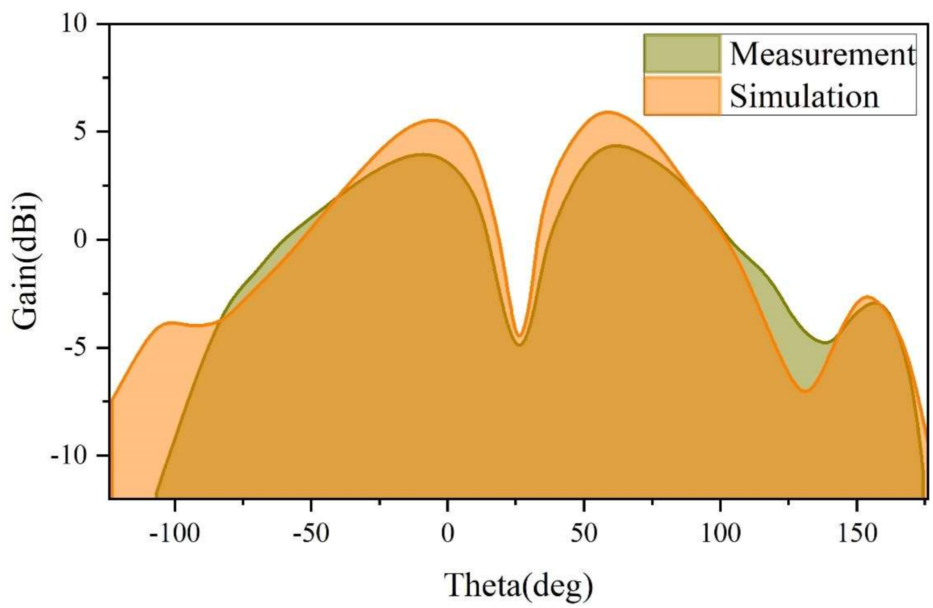

(b)Lower level feed network

Fig. 8. Circular patch test direction

4.2. Basic plasma theory

4.2.1. Numerical analysis. Gas discharge is a method of generating plasma, often used in engineering and laboratories. This method is to apply an external electric field to the electrons, so that they accelerate and collide with the neutral molecules of the gas, the gas is excited and ionized to produce plasma. Therefore, the magnitude of the applied voltage determines the magnitude of the plasma electron density, in order to facilitate the analysis, the relationship between the applied voltage and the plasma electron density is expressed by the following formula:

$$n_e \approx \left(-0.02U^2 + 0.4U - 0.06\right) \times 10^{17} m^{-3} \tag{34}$$

4.2.2. Analyzing results. In the experiment, the range of the optimal applied voltage for quantum state transport is generally 1.05V-9.98V, which is calculated by the UQAOA algorithm, and if the voltage is too high, it will be detrimental to the instrument. So according to the formula (34) can be obtained the applied voltage and electron density of the corresponding relationship graph shown in Figure 9, and because the plasma frequency is only related to the electron density, so you can get the relationship between the plasma density and the plasma frequency of the plasma density and the plasma frequency of the plasma density and the plasma frequency of the plasma density and the plasma frequency in the figure.

As can be seen from the figure, the corresponding plasma density ranges from $0.34014\times10^{17}\,\text{cm}^{-3}$ to $1.95793\times10^{17}\,\text{cm}^{-3}$, and the corresponding plasma frequency is from 1.65264 GHz to 3.94591 GHz.

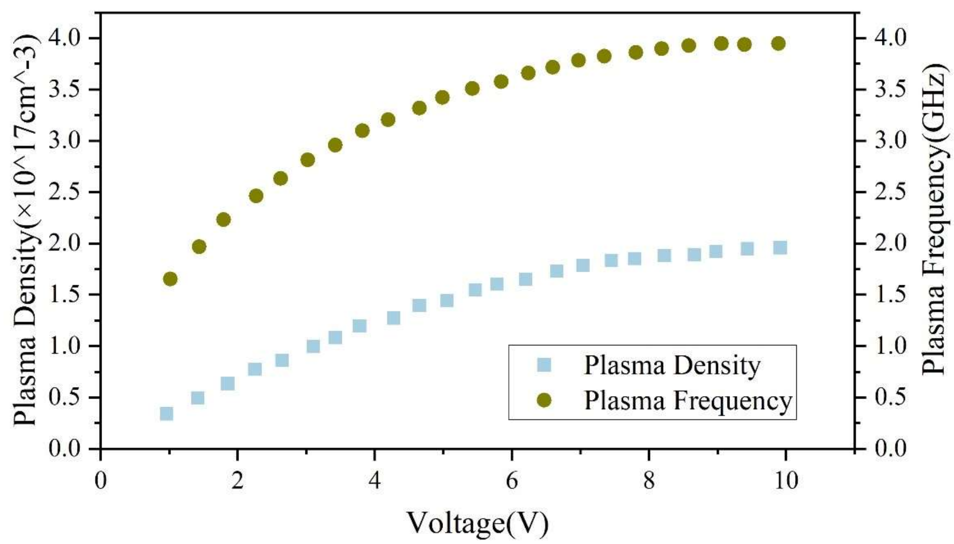

Fig. 9. The applied voltage corresponds to the plasma electron density and plasma frequency

Firstly, the homogeneous plasma is studied to analyze the effect of different plasma electron densities on the attenuation coefficient of electromagnetic wave, which is calculated by UQAOA algorithm after fixing the collision frequency at 0.45 GHz, and selecting the applied voltages as 2V, 3.5V, 5.5V and 9.5V, i.e., plasma electron densities of $0.66\times10^{17}\,\text{cm}^{-3}$, $1.2\times10^{17}\,\text{cm}^{-3}$, $1.5\times10^{17}\,\text{cm}^{-3}$ and $1.9\times10^{17}\,\text{cm}^{-3}$ respectively. After the calculation of UQAOA algorithm, the variation of attenuation coefficients with the incident wave frequency can be obtained under different plasma electron densities as shown in Fig. 10. When the plasma electron density is larger, the attenuation coefficient varies with the incident wave frequency more and slower, e.g., $n_e = 1.9\times10^{17}\,\text{cm}^{-3}$, which is close to 0 only when the incident wave frequency is 4 GHz.

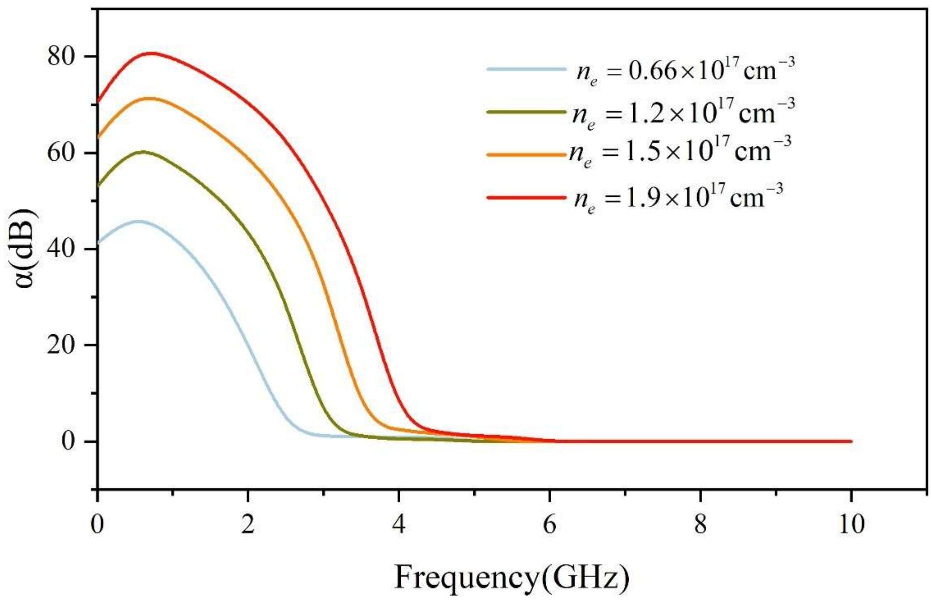

Fig. 10. Variation of attenuation coefficient with incident wave frequency at different electron

Next, we analyze the effect of different plasma collision frequencies on the attenuation coefficient of electromagnetic wave, based on the UQAOA algorithm, fix the plasma electron density as 1.2 $\times10^{17}\,\text{cm}^{-3}$, and select the collision frequencies as 0.45 GHz, 2 GHz, 5 GHz and 10 GHz.After calculation, we can get the change of the attenuation coefficient with the frequency of the incident wave under different plasma collision frequencies, as shown in Fig. 11.

From Fig. 11, it can be seen that when the incident wave frequency is small, the attenuation is larger as the collision frequency decreases, while as the incident wave frequency increases, the attenuation starts to behave diametrically opposite to that at low frequencies, i.e., the attenuation is larger as the collision frequency increases. For example, the attenuation coefficient of $\upsilon_c = 10GHz$, the second band of attenuation begins to occur at a frequency of 3.864. This is because, in the lower frequency band, the electrons in the plasma are not sufficiently accelerated to collide with other particles due to the effect of the incident electromagnetic wave. In the higher frequency band, as the plasma collision frequency increases, the electrons are frequently accelerated to collide with other particles to exchange energy, and the attenuation is also greater.

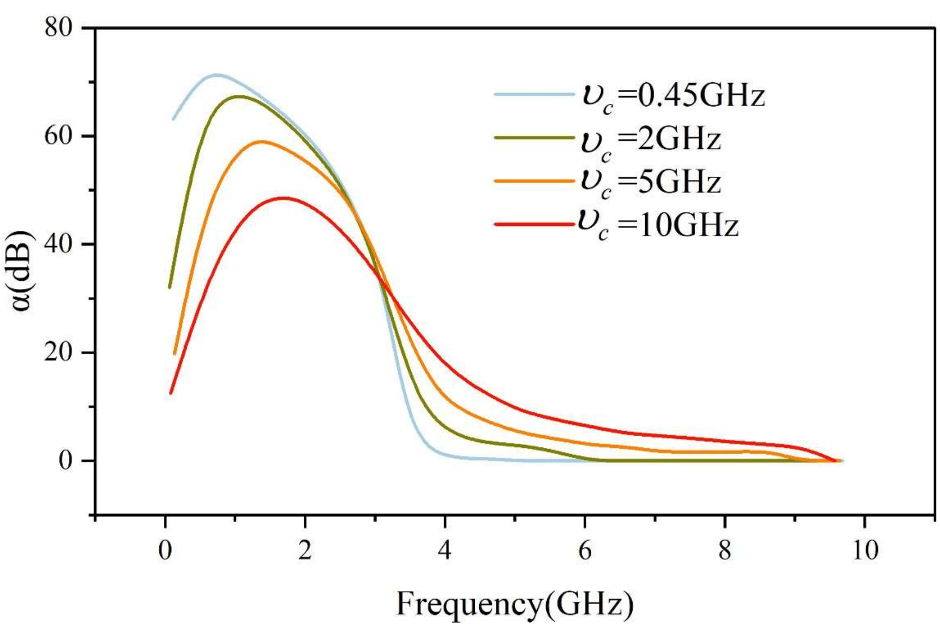

Fig. 11. The attenuation coefficient depends on the incident wave frequency at different collision

5. Conclusion

In this paper, the quantum entanglement effect is divided into two aspects, quantum state transmission and entanglement exchange, and the quantum entanglement research of electromagnetic waves is carried out from these two aspects respectively. The workflow of quantum approximation optimization algorithm is sorted out, and the quadratic unconstrained binary optimization method is proposed to solve the constraint problem of quantum state transmission.

In gives a treatment of the constrained mixed Hamiltonian quantity problem within the QAOA framework and evaluates the performance of the UQAOA algorithm on the Graph Partition problem. The UQAOA algorithm achieves better performance in the Graph Partition problem, with the approximation ratio remaining around 1 after the level number P = 4.

The UQAOA algorithm is used to analyze the change of compression parameters and effective coupling strength when quantum entanglement of electromagnetic waves occurs. It is found that the entanglement E_{ab} and E_{cm} increases and then decreases as G_c becomes larger. E_{cm} reaches a maximum value of 0.155 when G_c is 1.

Based on the UQAOA algorithm to analyze the transmission characteristics of the generated OMA waves in air and transmission optimization problem, the reflection coefficient obtained is slightly lower than the test, and the maximum error error is controlled at about ±7.5 dB, although the two results basically match. Meanwhile, in the test direction, in the lower feeder network, the maximum error is about ±2.5, and the error is within the acceptable range.

References

[1] Makarov, D. N. (2018). Quantum entanglement of a harmonic oscillator with an electromagnetic field. Scientific Reports, 8(1), 8204.

[2] Feng, D. (2019, March). Review of quantum navigation. In IOP Conference Series: Earth and Environmental Science (Vol. 237, p. 032027). IOP Publishing.

[3] You, J., Ma, Q., Zhang, L., Liu, C., Zhang, J., Liu, S., & Cui, T. (2023). Electromagnetic metamaterials: From classical to quantum. Electromagnetic Science, 1(1), 1-33.

[4] Zhao, S. R. (2023). Experiment to prove the existence of the advanced wave and experiment to prove the wrong definition of magnetic field in maxwell’s theory. International Journal of Physics, 11(2), 73-80.

[5] Paneru, D., Cohen, E., Fickler, R., Boyd, R. W., & Karimi, E. (2020). Entanglement: quantum or classical?. Reports on Progress in Physics, 83(6), 064001.

[6] Zloshchastiev, K. G. (2016). Quantum-statistical approach to electromagnetic wave propagation and dissipation inside dielectric media and nanophotonic and plasmonic waveguides. Physical Review B, 94(11), 115136.

[7] Chew, W. C., Liu, A. Y., Salazar-Lazaro, C., & Sha, W. E. (2016). Quantum electromagnetics: A new look—Part I. IEEE Journal on Multiscale and Multiphysics Computational Techniques, 1, 73-84.

[8] Defienne, H., Bowen, W. P., Chekhova, M., Lemos, G. B., Oron, D., Ramelow, S., ... & Faccio, D. (2024). Advances in quantum imaging. Nature Photonics, 18(10), 1024-1036.

[9] Safaei Bezgabadi, A., Borhani Zarandi, M., & Bolorizadeh, M. A. (2020). A quantum approach to electromagnetic wave propagation inside a dielectric. The European Physical Journal Plus, 135(8), 1-22.

[10] Qu, K., & Fisch, N. J. (2024). Producing entangled photon pairs and quantum squeezed states in plasmas.

Physical Review E, 110(6), 065211.

[11] Livreri, P., Galvano, B., Fasolo, L., Oberto, L., & Enrico, E. (2024). Josephson Traveling Wave Parametric Amplifier as Quantum Source of Entangled Photons for Microwave Quantum Radar Applications. ELECTROMAGNETIC WAVES, 179, 113-124.

[12] Wang, K., Chekhova, M., & Kivshar, Y. (2022). Metasurfaces for quantum technologies. Physics Today, 75(8), 38-44.

[13] Wong, B. (2019). On quantum entanglement. International Journal of Automatic Control System, 5(2), 1-7.

[14] Zhang, L., Li, Z., Liu, D., Wu, C., Xu, H., & Li, Z. (2023). Entangled x-ray photon pair generation by free-electron lasers. Physical Review Letters, 131(7), 073601.

[15] Maccone, L., & Ren, C. (2020). Quantum radar. Physical Review Letters, 124(20), 200503.

[16] Wen, X. G. (2018). Four revolutions in physics and the second quantum revolution—A unification of force and matter by quantum information. International Journal of Modern Physics B, 32(26), 1830010.

[17] Ma, Y., Miao, H., Pang, B. H., Evans, M., Zhao, C., Harms, J., ... & Chen, Y. (2017). Proposal for gravitational-wave detection beyond the standard quantum limit through EPR entanglement. Nature Physics, 13(8), 776-780.

[18] Wharton, K., & Adlam, E. (2023). Entangled Photon Anti-Correlations Are Evident from Classical Electromagnetism. Symmetry, 15(8), 1539.

[19] Lindel, F., Herter, A., Gebhart, V., Faist, J., & Buhmann, S. Y. (2024). Entanglement harvesting from electromagnetic quantum fields. Physical Review A, 110(2), 022414.

[20] Ji, W., Chang, J., Xu, H. X., Gao, J. R., Gröblacher, S., Urbach, H. P., & Adam, A. J. (2023). Recent advances in metasurface design and quantum optics applications with machine learning, physics-informed neural networks, and topology optimization methods. Light: Science & Applications, 12(1), 169.

[21] Peng, F., & Chen, X. (2024). A Fast Antenna Optimization Method Based on Mixed Quantum Entangled States. IEEE Transactions on Antennas and Propagation.

[22] Ram, A. K., Vahala, G., Vahala, L., & Soe, M. (2021). Reflection and transmission of electromagnetic pulses at a planar dielectric interface: Theory and quantum lattice simulations. AIP Advances, 11(10).

[23] Kono, S., Koshino, K., Tabuchi, Y., Noguchi, A., & Nakamura, Y. (2018). Quantum non-demolition detection of an itinerant microwave photon. Nature Physics, 14(6), 546-549.

[24] Konrad, T., & Forbes, A. (2019). Quantum mechanics and classical light. Contemporary Physics, 60(1), 1-22.

[25] De Fabritiis Philipe,Guedes Fillipe M.,Peruzzo Giovani & Sorella Silvio P. (2023). Entangled coherent states and violations of Bell-CHSH inequalities. Physics Letters A.

[26] Yu. Palii ,A. Bogolubskaya& D. Yanovich. (2024). Quantum Approximation Optimization Algorithm for the Ising Model in an External Magnetic Field. Physics of Particles and Nuclei(3),600-602.

[27] Yuma Hirakui & Takahiro Yajima. (2024). Applications of the Kosambi–Cartan–Chern Theory to Hamiltonian Systems on a Cotangent Bundle: Linking Geometric Quantities to the Self-Similar Motions of Three Point Vortices. Mathematics(1),126-126.

[28] Sadeghi Elham & Rezania Hamed. (2023). The effects of spin–orbit coupling on optical properties of electronic Lieb lattice in the presence of magnetic field. Solid State Communications.

[29] Shuji Watanabe. (2025). The BCS-Bogoliubov gap equation with external magnetic field and the first-order phase transition. Journal of Physics A: Mathematical and Theoretical(4),045203-045203.